

Magnetic structure of the frustrated $S = \frac{1}{2}$ chain magnet LiCu_2O_2 doped with nonmagnetic ZnA. A. Bush,¹ N. Büttgen,² A. A. Gippius,^{2,3} V. N. Glazkov,^{4,5} W. Kraetschmer,² L. A. Prozorova,⁴ L. E. Svistov,^{4,*}
A. M. Vasiliev,⁴ and A. Zheludev⁵¹Moscow State Technical University of Radioengineering, Electronics and Automation, 119454 Moscow, Russia²Center for Electronic Correlations and Magnetism EKM, Experimentalphysik V, Universität Augsburg, D-86135 Augsburg, Germany³Faculty of Physics, M.V. Lomonosov Moscow State University, 119899 Moscow, Russia⁴P. L. Kapitza Institute for Physical Problems RAS, 119334 Moscow, Russia⁵Neutron Scattering and Magnetism, Laboratory for Solid State Physics, ETH Zürich, Switzerland, 8093 Zürich, Switzerland

(Received 31 October 2012; revised manuscript received 21 August 2013; published 13 September 2013)

We present the results of magnetization, electron spin resonance (ESR), and nuclear magnetic resonance (NMR) measurements on single-crystal samples of the frustrated $S = 1/2$ chain cuprate LiCu_2O_2 doped with nonmagnetic Zn^{2+} . As shown by the x-ray techniques, the crystals of $\text{Li}(\text{Cu}_{1-x}\text{Zn}_x)_2\text{O}_2$ with $x < 0.12$ are single-phase, whereas for higher Zn concentrations the samples were polyphase. ESR spectra for all monophasic samples ($0 \leq x < 0.12$) can be explained within the model of a planar spin structure with a uniaxial type anisotropy. The NMR spectra of the highly doped single-crystal sample $\text{Li}(\text{Cu}_{0.9}\text{Zn}_{0.1})_2\text{O}_2$ can be described in the frame of a planar spin-glass-like magnetic structure with short-range spiral correlations in the crystal ab planes with strongest exchange bonds. The value of magnetic moments of Cu^{2+} ions in this structure is close to the value obtained for undoped crystals: $(0.8 \pm 0.1) \mu_B$.

DOI: 10.1103/PhysRevB.88.104411

PACS number(s): 75.50.Ee, 76.60.-k, 75.10.Jm, 75.10.Pq

I. INTRODUCTION

LiCu_2O_2 is an example of an $S = 1/2$ magnet with frustrated exchange interactions. The magnetic structure of LiCu_2O_2 can be considered as a system of coupled $S = 1/2$ chains of magnetic Cu^{2+} ions. Within the chains, the nearest spins interact ferromagnetically and the next-nearest neighbors antiferromagnetically. Interest in magnetic systems with such a type of frustration is stimulated by theoretical predictions of unusual magnetic phases for uncoupled and weakly coupled (1D and quasi-1D) chain models (see, for example, Refs. 1 and 2). It was shown that a new type of magnetic ordering can be realized for the magnets with this particular type of frustration. Such a type of magnetic order, with zero average magnetic moment on each magnetic ion, but with long-range ordered correlations of spin components of neighboring ions, is classified as spin-nematic order.³ The possibility to find this new type of magnetic order experimentally is a very attractive task. According to Ref. 1, for the 1D model with the intrachain exchange constants of LiCu_2O_2 , a chiral long-range order in the low-field range and a quasi-long-range ordered spin-density-wave phase in higher applied magnetic fields H are expected. In the experiment, the planar spiral spin structure was observed at $T < T_N$ in the low-field range in LiCu_2O_2 .^{4,5} At higher fields, $\mu_0 H \approx 15$ T, another magnetic phase, which is not identified yet, was observed.⁶ Probably, this phase is related to a spin-density-wave phase, which is predicted for the 1D model. A spin-nematic phase for the exchange integrals of LiCu_2O_2 is expected in even higher magnetic fields, which are hardly accessible experimentally.

Introduction of nonmagnetic impurities substituting for the magnetic ions provides a powerful tool to fine tune properties of the bulk magnet and to affect stability of different phases or even to stabilize new phases. The effect of nonmagnetic doping was studied in the collinearly ordered magnets (e.g., Refs. 7 and 8), in the quantum magnets (e.g., Refs. 9 and 10). Recent publications (e.g., Refs. 11–14) have

discussed the effect of nonmagnetic impurities on the matrix with frustrated interactions. Quasi-one-dimensional frustrated magnets are appealing objects for the study of such doping effects: first, breaking up the spin chain by an impurity can lead to the formation of the lengthy multispin defect with unusual properties.¹⁵ Besides, in the presence of the strong next-nearest-neighbor interaction unaffected by doping, substitution of the magnetic ion by nonmagnetic ones results in the conservation of the magnetic correlations along the chain with the defined spin spiral phase shift at the impurity location, while due to the random location of the defects, weak interchain interaction becomes frustrated.

The magnetometric and calorimetric investigations of the zinc-doped crystals of LiCu_2O_2 were reported recently¹⁶ and new magnetic phases in this system were announced. This report has stimulated the electron spin resonance (ESR) and nuclear magnetic resonance (NMR) investigations of the magnetic structure of Zn-doped LiCu_2O_2 single crystals reported here. Our x-ray, ESR, and NMR research provides no support for the existence of the dimer phase at doping levels above $x \approx 5\%$, suggested by Hsu *et al.*¹⁶ On the contrary, we have found that at the doping up to 10%, the resonance response of the system remains qualitatively similar to that of the pure sample and can be understood in terms of planar noncollinear structure. The NMR study of the $\text{Li}(\text{Cu}_{1-x}\text{Zn}_x)_2\text{O}_2$ single crystal with $x = 0.1$ at $T < T_N$ shows coexistence of static correlations corresponding to the magnetic structure of the undoped material with a static random distribution of spin directions. The temperature evolution of NMR spectra can be described by the development of the interplane correlations with decrease of the temperature. For the temperatures $T_N/2 < T < T_N$, the NMR spectra can be described in the model of uncorrelated ab spin planes.

The paper is built as follows. In Sec. II, a short overview of the literature data about the crystal and magnetic structures of the undoped samples of LiCu_2O_2 is given. In Sec. III,

the details of crystal growth and sample characterization are described. In Secs. IV and V, results of ESR and NMR experiments are presented.

II. CRYSTALLOGRAPHIC AND MAGNETIC STRUCTURES OF LiCu_2O_2

LiCu_2O_2 crystallizes in an orthorhombic system (space group $Pnma$) with unit cell parameters $a = 5.73 \text{ \AA}$, $b = 2.86 \text{ \AA}$, and $c = 12.42 \text{ \AA}$.¹⁷ The unit cell parameter a is approximately twice the unit cell parameter b . Consequently, the LiCu_2O_2 samples, as a rule, are characterized by twinning due to the formation of crystallographic domains rotated by 90° around their common crystallographic c axis.

The unit cell of the LiCu_2O_2 crystal contains four univalent nonmagnetic Cu^+ cations and four divalent Cu^{2+} cations with spin $S = 1/2$. There are four crystallographic positions of the magnetic Cu^{2+} ions in the crystal unit cell of LiCu_2O_2 , conventionally denoted as α , β , γ , and δ .

The Cu^{2+} ions in different positions are weakly magnetically coupled and form four almost independent systems of spin chains. Such chains formed by one of four kinds of Cu^{2+} ions (e.g., the α position) and relevant exchange interactions¹⁸ within the system are shown schematically in Fig. 1(a).

The positions of Cu^{2+} and Li^+ ions in the crystal cell are given¹⁷ by following copper coordinates: (0.876; 0.75; 0.095), (0.376; 0.75; 0.405), (0.624; 0.25; 0.595), and (0.124; 0.25; 0.905); and by lithium coordinates (0.376; 0.75; 0.068), (0.876; 0.75; 0.432), (0.124; 0.25; 0.568), and (0.624; 0.25; 0.932). Schematic arrangement of the Cu^{2+} and Li^+ ions in the projection of the crystal lattice onto the ac plane is given in Fig. 1(b).

The transition into the magnetically ordered state occurs via two stages at $T_{c1} = 24.6 \text{ K}$ and $T_{c2} = 23.2 \text{ K}$.¹⁹ Neutron scattering and NMR experiments have revealed that an incommensurate magnetic structure is realized in the magnetically ordered state ($T < T_{c1}$).^{4,5,20} The wave vector of the incommensurate magnetic structure coincides with the chain direction (the b axis). The magnitude of the propagation vector at $T < 17 \text{ K}$ is almost temperature independent and is equal to $0.827 \times 2\pi/b$. The neutron scattering experiments have shown that the neighboring magnetic moments along the a direction are antiparallel, whereas those along the c direction are parallel. The investigation of the spin-wave spectra by inelastic neutron scattering¹⁸ shows that the incommensurate magnetic structure in LiCu_2O_2 is caused by a competition between the ferromagnetic exchange interaction of the nearest-neighbor magnetic ions in the chain, $J_1 = -7.00 \text{ meV}$, and the antiferromagnetic interaction of the next-nearest-neighbor ions in the chain, $J_2 = 3.75 \text{ meV}$. The antiparallel orientation of the magnetic moments of Cu^{2+} between neighboring chains is caused by the strong antiferromagnetic interaction $J_3 = 3.4 \text{ meV}$. The coupling of the Cu^{2+} magnetic moments along the c direction and the couplings between the magnetic ions in different crystallographic positions α , β , γ , or δ are much weaker.^{5,18} Thus the magnetic structure of LiCu_2O_2 in the magnetically ordered phase can be considered as quasi-two-dimensional. The quasi-two-dimensional character of the magnetic interactions in LiCu_2O_2 was also proven by resonant soft x-ray magnetic scattering experiments.^{21,22}

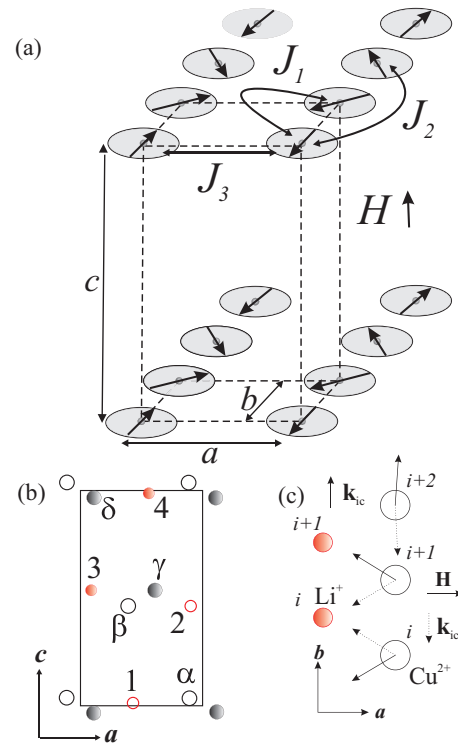


FIG. 1. (Color online) (a) Schematic representation of the arrangement of Cu^{2+} moments in LiCu_2O_2 . Only one of four Cu^{2+} (α , β , γ , δ) positions is shown. Arrows correspond to the spin directions below T_{c2} for $\mathbf{H} \parallel \mathbf{c}$. J_1 , J_2 , and J_3 are the main exchange integrals.¹⁸ (b) Schematic arrangement of the Cu^{2+} and Li^+ ions in the projection of the crystal lattice onto the ac plane.²³ Large circles indicate the Cu^{2+} ions and small circles are the Li^+ ions. Closed and open circles represent ions with the coordinates equal to $0.25b$ and $0.75b$ along the b axis, respectively. (c) Sketch of the spin configuration corresponding to the extreme values of dipolar fields at Li site for two incommensurate domains with incommensurability vector directed up (solid arrows) or down (dashed arrows) chain. All spin vectors and the external field are in plane of figure.

The magnetic structure of LiCu_2O_2 at zero magnetic field was studied using different experimental methods, but so far there is no generally accepted model for it. For a review of proposed models see, for example, Ref. 6.

In magnetic fields above 3 T, the magnetic structure realized in LiCu_2O_2 is much clearer. ESR and NMR studies of LiCu_2O_2 in the low-temperature magnetically ordered phase ($T < T_{c2}$) established that a planar spiral magnetic structure is formed in this compound.²³ The magnetic moments located at the α (β , γ , or δ) position of the crystal unit cell with coordinates x , y , z (measured along the \mathbf{a} , \mathbf{b} and \mathbf{c} axes of the crystal, respectively) are defined as

$$\begin{aligned} \boldsymbol{\mu}_\alpha = & \mu \mathbf{l}_1 (-1)^{x/a} \cos(k_{ic} y + \phi_\alpha) \\ & + \mu \mathbf{l}_2 (-1)^{x/a} \sin(k_{ic} y + \phi_\alpha), \end{aligned} \quad (1)$$

where \mathbf{l}_1 and \mathbf{l}_2 are the two mutually perpendicular unit vectors, \mathbf{k}_{ic} is the incommensurability vector parallel to the chain direction (b axis), μ is the magnetic moment of the Cu^{2+} ion, and x is a multiple of the chain period a . The magnetic moment per copper ion at $T \lesssim 10 \text{ K}$ was evaluated as $\mu = 0.85 \mu_B$.^{4,23} The phases ϕ_α , ϕ_β , ϕ_γ , and ϕ_δ determine the mutual orientation

of the spins in the chains formed by the ions in the different crystallographic positions. Their values are extracted from the NMR data:^{23,24} $\phi_\alpha = 0$, $\phi_\beta = \phi_\alpha + \pi/2$, $\phi_\gamma = \pi - k_{ic}b/2$, and $\phi_\delta = \phi_\gamma + \pi/2$.

III. SAMPLE PREPARATION AND EXPERIMENTAL DETAILS

Single crystals of $\text{Li}(\text{Cu}_{1-x}\text{Zn}_x)_2\text{O}_2$ with the size of several cubic millimeters were prepared by the “solution-in-the-melt” method.²⁵ Samples were grown in air by a flux method in alundum crucibles. The mixtures of analytical grade Li_2CO_3 , CuO and ZnO of $\text{Li}_2\text{CO}_3 \cdot 4(1-x)\text{CuO} \cdot 4x\text{ZnO}$ compositions were melted at 1100°C , and then solidified by cooling to 930°C at a rate of $5.0^\circ\text{C}/\text{hour}$. Next, the crucible was withdrawn from the furnace and placed on a massive copper plate to ensure rapid cooling to room temperature. Quenching from $\approx 900^\circ\text{C}$ was necessary, because the single phase LiCu_2O_2 single crystals decompose below this temperature.²⁵

The samples were shaped as a flat plates with the developed ab plane. The twinning structure of the samples was studied with optical polarization microscopy.⁶ In most cases, the samples were twinned with a characteristic domain size of several microns. It was possible to select samples without twinning structure for Zn concentrations up to $x = 0.1$. The absence of the twinning structure in the samples selected for the experiments was confirmed by x-ray diffraction and ESR measurements.^{6,23} We have used samples without twinning for most of the experiments described below.

The x-ray diffraction patterns were taken in a θ - 2θ geometry using $\text{CuK}\alpha$ irradiation. The samples produced clearly distinguishable diffraction patterns from the bc and the ac planes of the crystal. The spectra obtained from twinned samples had a form of a superposition of these spectra. The Zn doping of LiCu_2O_2 results in a monotonic change of the cell parameters up to a concentration limit of $x_c \approx 0.12$. For samples with zinc content of initial charge $x < 0.12$, no diffraction patterns due to impurity phases were observed. Additional x-ray diffraction patterns were observed for the samples with $x \geq 0.12$, which can be ascribed to the presence of inclusions of impurity phases. The patterns ascribed to the main phase show that the cell parameters for higher Zn content do not change. The zinc concentrations of $\text{Li}(\text{Cu}_{1-x}\text{Zn}_x)_2\text{O}_2$ single crystals were measured by electron probe micro analysis on the spectrometer “Eagle II” (“EDAX”, USA). The concentration values of x in our single-crystalline samples obtained with this method coincide with the values x_0 of the zinc concentration in the initial charge with precision better than $x_0 \pm 0.03$ for all samples with $x < x_c$.

The dependence of the crystal cell parameters a, b, c of the single crystals of $\text{Li}(\text{Cu}_{1-x}\text{Zn}_x)_2\text{O}_2$ on zinc concentration x in initial charge is shown in Fig. 2. The solid symbols show the results obtained from the samples described above. In contrast with the data of Ref. 16 (open symbols), we did not observe any anomaly in the concentration dependence of the cell constants at $x = 0.055$.

Magnetization curves in static magnetic fields of up to 7 T were measured with a commercial superconducting quantum interference device (SQUID) magnetometer (Quantum Design MPMS-XL7).

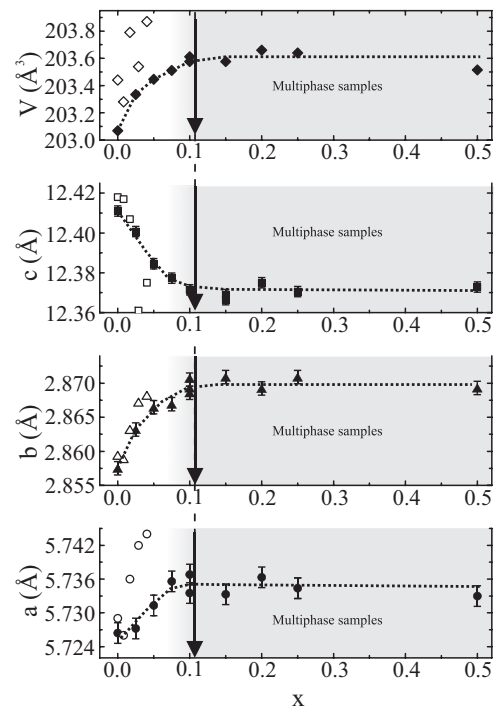


FIG. 2. The concentration dependence of the crystal unit cell volume (top) and crystal unit cell parameters a, b, c (lower) of single crystals of $\text{Li}(\text{Cu}_{1-x}\text{Zn}_x)_2\text{O}_2$. x is a concentration of zinc in initial charge. The solid symbols show the results obtained on our samples discussed here. The open symbols show the data taken from Ref. 16.

The ESR experiments were performed with a transmission-type spectrometer using resonators in the frequency range $18 < \nu < 120$ GHz. The magnetic field of a superconducting solenoid was varied in the range of $0 < \mu_0 H < 8$ T. Temperatures were varied within the range of $1.2 < T < 30$ K.

The NMR experiments were performed with a conventional phase coherent, homemade pulse spectrometer at a fixed frequency of $\nu = 61$ MHz. We investigated the ${}^7\text{Li}$ ($I = 3/2$, $\gamma/2\pi = 16.5466$ MHz/T) nuclei using spin-echo technique with a pulse sequence $5 \mu\text{s} - \tau_D - 10 \mu\text{s}$, where the time between pulses τ_D was $40 \mu\text{s}$. The spectra were collected by sweeping the applied magnetic field between $3.5 < \mu_0 H < 3.9$ T. The temperatures were stabilized with a precision better than 0.02 K.

IV. EXPERIMENTAL RESULTS

A. Magnetization measurements

The experimental curves $M(T)/H$ and their temperature derivatives for different field directions $\mathbf{H} \parallel \mathbf{a}, \mathbf{b}$ and $\mathbf{H} \parallel \mathbf{c}$ at $\mu_0 H = 0.1$ T are shown in Figs. 3 and 4. The dependencies were obtained on the single crystal without doping ($x = 0$) and on the twinned single crystal with $x = 0.1$. For all field directions, broad maxima of $M(T)/H$ were observed at $T = 38$ K for samples without doping and at $T = 31$ K for doped samples with $x = 0.1$. The maximum is typical for low-dimensional antiferromagnets. In the paramagnetic region, the magnetic susceptibility for $\mathbf{H} \parallel \mathbf{c}$ exceeds that for $\mathbf{H} \parallel \mathbf{a}, \mathbf{b}$, which is consistent with the anisotropy of the g tensor measured in the ESR experiments²⁶ ($g_{a,b} = 2.0$; $g_c = 2.2$). At

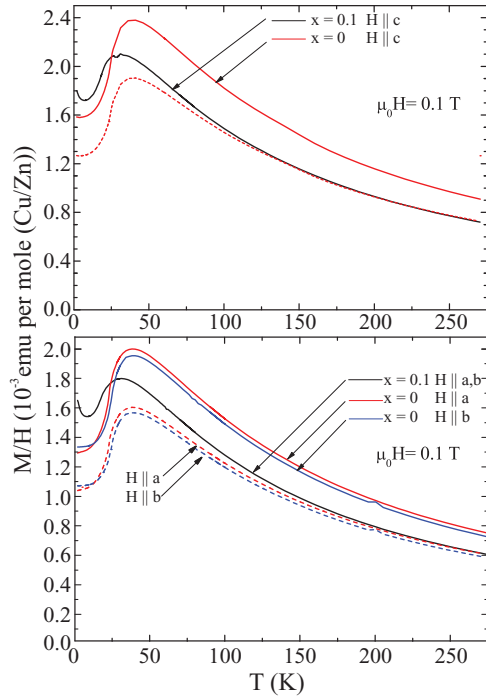


FIG. 3. (Color online) Temperature dependencies of the magnetic susceptibility $M(T)/H$ for field directions $\mathbf{H} \parallel \mathbf{c}$ (top) and $\mathbf{H} \parallel \mathbf{a}, \mathbf{b}$ (bottom) at $\mu_0 H = 0.1$ T. Susceptibility of the Zn-doped sample with $x = 0.1$ was measured on the twinned single crystal, data for the untwinned crystal with $x = 0$ at $\mathbf{H} \parallel \mathbf{a}, \mathbf{b}$ and \mathbf{c} are taken from Ref. 6. Dashed lines show the same $M(T)/H$ curves for undoped samples ($x = 0$), scaled on the y axis by a factor of $1 - 2x = 0.8$.

high temperatures $T \gtrsim 150$ K, the susceptibility of the doped sample is $(20 \pm 1.2)\%$ less than that of the pure sample. This reduction is close to the factor $(1 - 2x)$ expected if all Zn^{2+} ions take the places of the Cu^{2+} ions, which would result in the corresponding decrease of the number of paramagnetic spins. To emphasize this fact, the $M(T)/H$ dependence for the sample without doping reduced by factor 0.8 is shown in the same figure with dashed lines. This experiment allows to conclude that the number of magnetic Cu^{2+} ions in the doped samples of $\text{Li}(\text{Cu}_{1-x}\text{Zn}_x)_2\text{O}_2$ is reduced by the number of nonmagnetic Zn^{2+} ions.

The transitions to the magnetically ordered states at T_{c1} and T_{c2} are marked by the change of the $M(T)/H$ slope. These inflection points are well resolved in the temperature derivative of $M(T)/H$ for the undoped sample (see Fig. 4). The $(d/dT)[M(T)/H]$ curves are strongly anisotropic;⁶ for $\mathbf{H} \parallel \mathbf{b}$ and \mathbf{c} , there are two anomalies corresponding to two transitions at T_{c1} and T_{c2} . The temperature dependence of $(d/dT)[M(T)/H]$ for $\mathbf{H} \parallel \mathbf{a}$ shows only one sharp peak at the lower temperature near T_{c2} in the studied field range. For the doped sample, the inflection points on the $M(T)/H$ curves were smoothed, but the maximum of the slope for $\mathbf{H} \parallel \mathbf{c}$ was observed at evidently higher temperature than for $\mathbf{H} \parallel \mathbf{a}, \mathbf{b}$. The distance between the maxima for doped samples with $x < 0.1$ is almost the same as for the samples without doping (see Fig. 4). Thus the double-step transition in the magnetically ordered phase also takes place for doped samples. Note here that the double-stage transition is specific for a planar spin

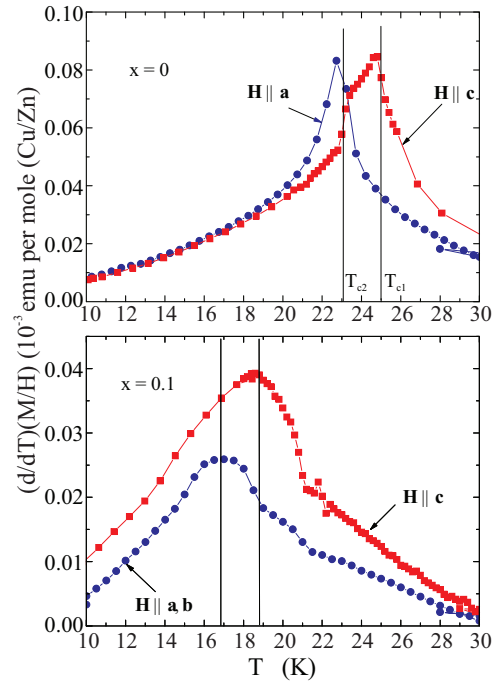


FIG. 4. (Color online) Temperature dependencies of the magnetization derivative dM/dT for field directions $\mathbf{H} \parallel \mathbf{a}, \mathbf{b}$ (circles) and \mathbf{c} (squares) and $\mu_0 H = 0.1$ T for the undoped untwinned crystal $x = 0$ (top, taken from Ref. 6) and for the twinned doped single crystals of $\text{Li}(\text{Cu}_{1-x}\text{Zn}_x)_2\text{O}_2$ with $x = 0.1$ (bottom). Data are obtained from $M(T)/H$ at $\mu_0 H = 0.1$ T.

structure with a strong easy-plane anisotropy for the vector \mathbf{n} normal to the spin plane. The anomaly of $M(H)$ at a field of $\mu_0 H_{c1} \approx 2$ T for $\mathbf{H} \parallel \mathbf{b}$, which was associated with the reorientation of the spin plane observed earlier for samples without doping⁶ was not observed for all studied samples with $x \geq 0.025$.

B. ESR experiments

The ESR in single crystals of $\text{Li}(\text{Cu}_{1-x}\text{Zn}_x)_2\text{O}_2$ was studied on the samples with $x = 0.025, 0.05, 0.075, 0.1$. The samples with $x = 0.025$ and 0.1 were untwinned. ESR on the sample without doping was studied in a previous work.²³ The typical ESR absorption lines are shown in the lower panels of Figs. 5 and 6. We present the lines for the samples with the Zn concentration $x = 0.075, 0.1$, and the undoped untwinned sample from Ref. 23. The ESR absorption lines are systematically broader for the samples with larger Zn concentration. The insert in the lower panel of Fig. 5 shows the concentration dependence of the absorption linewidth for $\mathbf{H} \parallel \mathbf{c}$ at $T = 4.2$ K. The ESR frequency-field dependencies $\nu(H)$ for field directions $\mathbf{H} \parallel \mathbf{c}, \mathbf{b}$ for the samples with $x = 0, 0.075$, and 0.1 are shown in the upper panels of Figs. 5 and 6. Note that for $\mathbf{H} \parallel \mathbf{c}$, the presence of the twinning is not essential. The sample with $x = 0.05, 0.075$ were twinned, but due to strong anisotropy (see below), it was easy to separate the absorption lines only from the domain with $\mathbf{H} \parallel \mathbf{b}$. The dash-dotted lines in the upper panels of Figs. 5 and 6 mark $\nu(H)$ dependencies of electron paramagnetic resonance for LiCu_2O_2 : $\nu = (g\mu_B/h)H$ ($g_{a,b} = 2.0$ and $g_c = 2.2$).²⁶

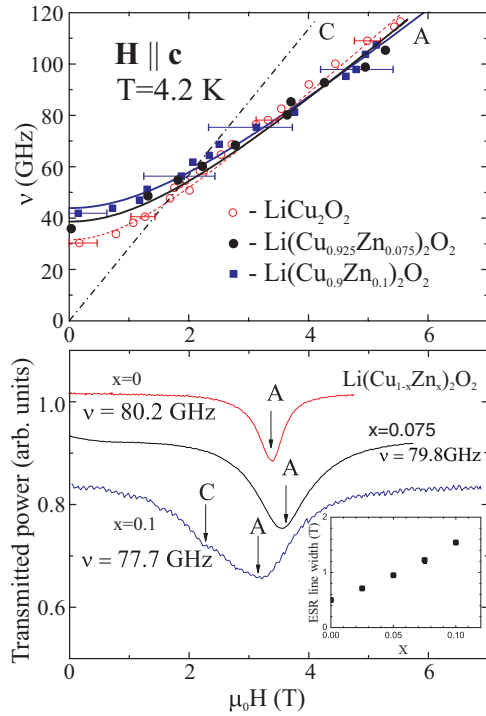


FIG. 5. (Color online) (Top) ESR frequency-field dependencies for $\text{Li}(\text{Cu}_{1-x}\text{Zn}_x)_2\text{O}_2$ samples with $x = 0.075, 0.1$ (black and blue solid symbols) and $x = 0$ (open symbols, from Ref. 23), $\mathbf{H} \parallel \mathbf{c}$, $T = 4.2$ K. Solid and dashed lines show fits with the equation given in the text. The dash-dotted line shows the spectra of the absorption component “C,” which coincides with the position of the paramagnetic absorption at $T > T_N$. (Bottom) Examples of ESR absorption spectra measured on three samples with $x = 0.1, 0.075$, and 0 at close frequencies ($\nu \approx 79$ GHz), $\mathbf{H} \parallel \mathbf{c}$, and $T = 4.2$ K. (Insert) Dependence of the “A”-component ESR linewidth on the Zn concentration. $\mathbf{H} \parallel \mathbf{c}$, $T = 4.2$ K, $\nu \approx 79$ GHz.

Resonance fields of the relatively weak component “C” are well described by such a paramagnetic dependence. Probably, this component is due to paramagnetic inclusions.

The experimental data which correspond to the absorption component “C” are not shown in the upper panels of Figs. 5 and 6. The ESR frequency-field dependencies [$\nu(H)$] of the intermediate Zn concentrations $x = 0.025, 0.05$ (not shown), and 0.075 interpolate between those of the samples with extreme doping concentration $x = 0$ and 0.1 . The error bars in the upper panels of Figs. 5 and 6 show the antiferromagnetic resonance linewidths measured at the half of the absorbed intensities.

The main features of the ESR frequency-field dependencies [$\nu(H)$] for different Zn concentrations remain the same as for the undoped sample. The frequency-field dependencies [$\nu(H)$] consist of a single branch for $\mathbf{H} \parallel \mathbf{c}$ and two branches for $\mathbf{H} \parallel \mathbf{b}$. In the case of pure compound, modes “A” and “B” were ascribed to the oscillations of the spin plane around a axis.²³ The sudden change of these mode resonance frequency at $\mathbf{H} \parallel \mathbf{b}$ at H_{c1} is associated with spin-flop transition.

The zero-field gap grows on doping from $\nu(H = 0) = 30 \pm 2$ GHz for the undoped sample ($x = 0$) to $\nu(H = 0) = 42 \pm 2$ GHz for doped samples with $x = 0.1$. Angular dependencies of the resonance fields on rotation in the ab plane for samples

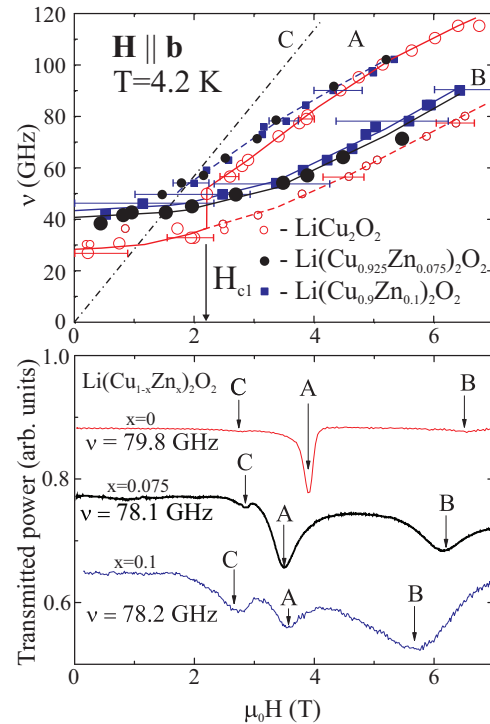


FIG. 6. (Color online) (Top) ESR frequency-field dependencies for $\text{Li}(\text{Cu}_{1-x}\text{Zn}_x)_2\text{O}_2$ samples with $x = 0.075, 0.1$ (black and blue solid symbols) and $x = 0$ (open symbols, from Ref. 23). Intense components are marked by large symbols, weak components are marked by small symbols, respectively, for $\mathbf{H} \parallel \mathbf{b}$, $T = 4.2$ K. The solid and dashed lines are guides to the eyes. The dash-dotted line corresponds to the absorption component “C,” which coincides with the EPR spectra measured at $T > T_N$. (Bottom) Example of field dependencies of the transmitted power, measured on three samples with $x = 0.1, 0.075$, and 0 at two close frequencies ($\nu \approx 79$ GHz), $\mathbf{H} \parallel \mathbf{b}$, and $T = 4.2$ K.

with $x = 0, 0.1$ are shown in Fig. 7. Both resonance fields shift to higher fields as \mathbf{H} approaches $\mathbf{H} \parallel \mathbf{a}$. Such a behavior was observed also for a rotation of the applied magnetic field H in the ac plane. Thus rotation of the static field towards

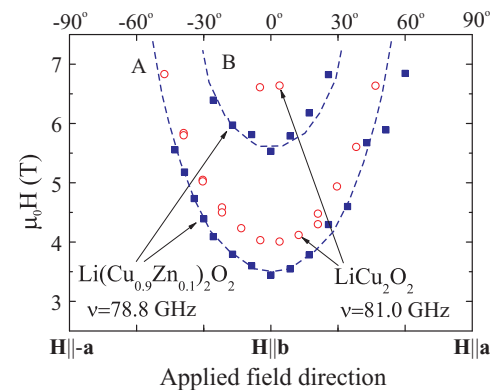


FIG. 7. (Color online) ab plane angular dependencies of the resonance fields for “A” and “B” components measured on $\text{Li}(\text{Cu}_{1-x}\text{Zn}_x)_2\text{O}_2$ samples with $x = 0.1$ (solid symbols) and $x = 0$ (open symbols) for frequencies around 80 GHz. $T = 4.2$ K. The dashed lines are guides to the eyes.

the \mathbf{a} direction flattens the $\nu(H)$ dependence, which finally becomes field independent for $\mathbf{H} \parallel \mathbf{a}$ (as was reported for the pure compound in Ref. 23). From these data, we conclude that the strong uniaxial anisotropy along the \mathbf{a} direction remains for all studied doped samples. Such an anisotropy corresponds to the easy bc plane anisotropy for the vector \mathbf{n} normal to the spin plane.

The branches marked as “A” for $\mathbf{H} \parallel \mathbf{c}$ are quasi linear with field: $\nu = k\sqrt{H^2 + \Delta^2}$. The coefficient k is noticeably smaller than the gyromagnetic ratio $g\mu_B/h$. Such a field dependence is typical for a planar spin structure with strong “easy-plane” anisotropy for vector \mathbf{n} perpendicular to the spin plane and field direction perpendicular to the anisotropy axis ($\mathbf{H} \perp \mathbf{a}$).²⁷ The coefficient k is defined by the anisotropy of the susceptibility of the spin structure: $k = (g\mu_B/h)\sqrt{(\chi_{\parallel}/\chi_{\perp} - 1)}$ (here, χ_{\parallel} and χ_{\perp} are the susceptibilities for field directions parallel and perpendicular to the vector \mathbf{n} of the spiral spin structure). Using the value of k as a fit parameter, we obtained that the anisotropy of the susceptibility $\chi_{\parallel}/\chi_{\perp} - 1$ slightly decreases from 0.55 ± 0.02 to 0.5 ± 0.02 with the increase of doping from $x = 0$ to 0.1.

For the field orientation $\mathbf{H} \parallel \mathbf{b}$, the magnetic structure of the undoped LiCu_2O_2 samples undergoes a reorientation at a field of $\mu_0 H_{c1} \approx 2$ T. Earlier experiments have shown that at this field the spin plane of the spiral structure rotates from the ab to the ac plane.^{6,23} The magnetic susceptibility at this field undergoes a steplike increase. The ESR frequency-field dependence for this orientation is shown in the upper panel of Fig. 6. The transition field H_{c1} is marked by the jump of the frequency-field dependence for the undoped sample. The intensive component of the ESR absorption line changes from the “B” branch of the frequency-field diagram to the “A” branch at the transition field H_{c1} for the undoped sample. Thus the “A” component dominates the absorption spectrum of the undoped sample at high fields (see Fig. 6). Observation of the weak absorption corresponding to the mode “B” above the spin-flop transition is probably due to the small areas where the spin plane is pinned. For the doped sample with $x = 0.1$, the absorption component “B” was more than ten times more intensive than the component “A” in the whole field range. No jumps of the position of the intense component in the frequency-field diagram was observed for the doped samples.

From these observations, we conclude that for doped samples no magnetic reorientation takes place in the studied field range. This conclusion is in agreement with the absence of anomalies in the $M(H)$ curves mentioned in the previous section. Note that the value of H_{c1} and the sharpness of the transition are strongly dependent on the quality of the samples even for the crystals without doping.^{6,23}

C. NMR experiments

The magnetic structure of the single crystals of $\text{Li}(\text{Cu}_{1-x}\text{Zn}_x)_2\text{O}_2$ with $x = 0.1$ was tested with the NMR technique. ^7Li NMR field-sweep spectra measured at different temperatures at field orientation $\mathbf{H} \parallel \mathbf{c}$ and fixed frequency $\nu = 61.0$ MHz are shown in Fig. 8. The shape of the NMR spectra transforms from a single component spectrum at high temperatures $T > T_N$ to a spectrum with characteristic shoulders at temperatures below $T_N \approx 18$ K (see Fig. 8).

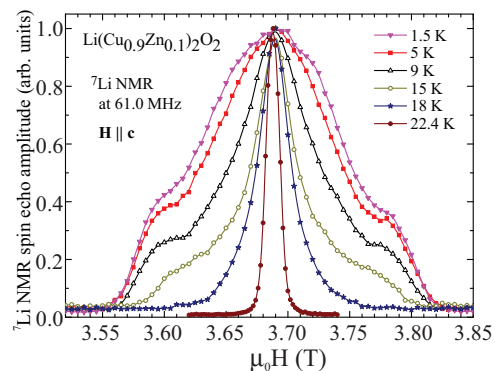


FIG. 8. (Color online) NMR spectra of ^7Li nuclei in $\text{Li}(\text{Cu}_{1-x}\text{Zn}_x)_2\text{O}_2$, $x = 0.1$, measured at different temperatures. $\mathbf{H} \parallel \mathbf{c}$ and pumping frequency $\nu = 61.0$ MHz.

Similar NMR spectra evolution was reported in Ref. 28 for the sample with Zn content $x = 0.029$.

The spin echo NMR signal in the low temperature range was observed in a broad field range $\mu_0 \Delta H \approx 0.25$ T, which is approximately the same as for LiCu_2O_2 without doping (see Fig. 9). At temperatures close to T_N , the central line of the NMR spectra dominates. This fact demonstrates that close to Neel temperature the number of nuclei with paramagnetic environment increases.

In Fig. 9, the lines show the fitting results of the NMR spectra. The ^7Li NMR spectra for doped and undoped samples were fitted by taking into account dipolar fields within the model of a planar spiral magnetic structure in the ab plane with an incommensurate wave vector $k_{ic} = 0.827 \times 2\pi/b$ aligned along the \mathbf{b} direction and an effective magnetic moment on the Cu^{2+} position equal to $0.8 \mu_B$. Note that the contribution of the contact field for such spin arrangement at $\mathbf{H} \parallel \mathbf{c}$ can be neglected since the spin plane is perpendicular to the magnetic field.²⁹ The magnetic structure for the sample without doping is described by Eq. (1). The mutual orientation of the spins from neighboring ab planes defined by phases $\phi_{\alpha,\beta,\gamma,\delta}$ are given in the end of Sec. II. The linewidth of individual groups of resonating lithium nuclei for this computation was taken as $\delta H = 0.005$ T, which is much smaller than all peculiarities on the experimental spectra. This value of δH roughly corresponds to the value of quadrupolar splitting of NMR line on ^7Li nuclei in LiCu_2O_2 ($\nu_q \approx 51.7$ kHz, Ref. 5).

To explain the main features of our experimentally observed NMR spectra we consider effective fields at lithium sites that are generated by an individual magnetic chain of Cu^{2+} ions nearest to the lithium nuclei [see the fragment of the spiral structure shown in Fig. 1(c)]. For simplicity, we suppose that the Li^+ ion, the Cu^{2+} chain, the spin vectors, and the applied static field \mathbf{H} lies in the plane of the figure. The projection of the effective field from neighboring spins on the applied field \mathbf{H} changes along the spin chain sinusoidally. For a given propagation vector k_{ic} the NMR spectra exhibit a shape with two characteristic maxima at the extremum fields $\nu/\gamma \pm H_{\text{ext}}$. Since the Li^+ ions are located symmetrically between two Cu^{2+} ions, the extreme fields H_{ext} will correspond to the arrangement of the spins in the copper chain symmetric with respect to the chosen Li^+ ion [marked with index i in Fig. 1(c)].

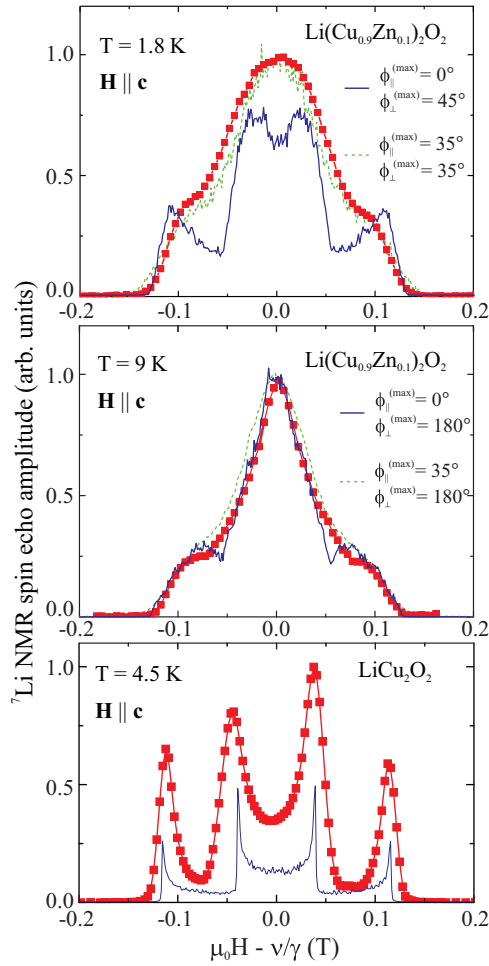


FIG. 9. (Color online) Squares represent NMR spectra of ${}^7\text{Li}$ nuclei in $\text{Li}(\text{Cu}_{1-x}\text{Zn}_x)_2\text{O}_2$, $x = 0.1$ (top and middle) and $x = 0$ (bottom) measured at $T < T_N$ for $\mathbf{H} \parallel \mathbf{c}$ and $\nu = 61.0$ MHz. The solid lines show the simulated spectra in models of spiral planar spin structures within the ab plane with long-range order in the \mathbf{c} direction for the undoped sample (bottom) and with disorder in the \mathbf{c} direction for the doped sample (top and middle). The dashed lines show the simulated spectra in the models of randomly disturbed planar spiral spin structure within ab planes with short-range order in \mathbf{c} direction (top and middle).

As it is schematically shown in Fig. 1(c), such a symmetric arrangement corresponding to the magnetic structures, with opposite wave vectors k_{ic} (solid arrows) and $-k_{ic}$ (dotted arrows), yields different dipolar contributions to effective field. Thus for such simple model structure, we can expect a broad NMR spectrum with four characteristic maxima corresponding to two magnetic domains with opposite wave vectors.

The magnetic structure expected for LiCu_2O_2 at an arbitrary orientation of the applied magnetic field provides NMR spectra with eight maxima corresponding to the four extremal fields at the lithium nuclei from different positions Li1, Li2, Li3, and Li4 [see Fig. 1(b)]. For the field orientation $\mathbf{H} \parallel \mathbf{c}$, the number of maxima of the spectra is reduced to four (see bottom panel of Fig. 9).

In order to interpret the NMR spectra of doped samples, we simulated the NMR spectra for the structures with random

static deviations of the spin directions from the spin orientations of undoped model. For modeling purposes, the deviation angles within the spin plane were set to the random value $-\phi^{(\max)} < \phi < \phi^{(\max)}$, where the maximal deviation $\phi^{(\max)}$ was used as a model fitting parameter. Taking into account that the exchange interactions between planes is weaker than the in-plane interactions, we used different deviation parameters $\phi_{\parallel}^{(\max)}$ for spins within ab plane and $\phi_{\perp}^{(\max)}$ for spins from different planes. The NMR spectra of doped samples at 9 K can be fitted in the model of totally random mutual orientation of the spins of the neighbor planes, i.e., $\phi_{\perp}^{(\max)} = 180^\circ$ (see middle panel of Fig. 9). The NMR spectra obtained in this model are only weakly sensitive to the disorder within the individual spin plane. The solid blue line shows the computed NMR spectra with the assumption of ordered moments within each ab plane ($\phi_{\parallel}^{(\max)} = 0^\circ$). The dashed green line shows NMR spectra obtained under the assumption that the spin directions of ions within the ab planes are oriented randomly around undisturbed directions within the angle $\phi_{\parallel}^{(\max)} = 35^\circ$. For the fit, we took $0.8 \mu_B$ as the absolute value of the magnetic Cu^{2+} moments at this particular temperature of $T = 9$ K. As temperature decreases the central maximum of the spectra starts to broaden (see Fig. 8). Such transformation can be explained by the development of spin correlations between ions of neighboring ab planes on cooling. The NMR spectrum measured at 1.8 K (squares) and the fitting results (lines) are given in the top panel of Fig. 9. Again, the solid blue line shows the computed NMR spectrum with the assumption of ordered moments within each ab plane ($\phi_{\parallel}^{(\max)} = 0^\circ$) and random deviations of nearest spins from neighboring planes within the angle $\phi_{\perp}^{(\max)} = 45^\circ$. A better agreement between our model and the low-temperature experimental NMR spectrum is obtained for the case of a magnetic structure with short ranged static correlations for both in-plane and interplane correlations according to the green dashed line. It shows the computed NMR spectrum with the assumption of random deviations of spins described by the parameters $\phi_{\parallel}^{(\max)} = \phi_{\perp}^{(\max)} = 35^\circ$. Again, the absolute value of the magnetic moments of Cu^{2+} was taken to be $0.8 \mu_B$ for the fit.

Finally, we must note that the local field at the probing nuclei is defined mostly by four nearest coordination spheres, which means that the NMR spectra are testing the short-range static correlations only. These correlations must be static at least during the time window of ≈ 0.1 s set by our NMR experiment. Thus the simulation does not actually rely on the assumption of the long-range order, and the same results can be obtained if we assume presence of only short-range order superimposed by the static random variations.

V. DISCUSSION

X-ray diffraction and electron probe micro analysis of the single-phase crystals of $\text{Li}(\text{Cu}_{1-x}\text{Zn}_x)_2\text{O}_2$ show that Zn ions enter into the lattice without destruction of the crystal structure in the broad concentration range $0 \leq x \lesssim 0.12$. The scaling of the high-temperature susceptibility as $(1 - 2x)$, shown in the Fig. 2, indicates that Zn ions substitute for Cu^{2+} and each Zn^{2+} ion reduces the number of magnetic ions by one. Nonmagnetic

dilution should also affect the effective interspin interactions (i.e., Curie-Weiss temperature Θ). The fit of our $H \parallel c$ susceptibility data in the 150–300 K temperature range shows that the Curie-Weiss temperature decreases from (61 ± 3) K for the pure compound to (51 ± 5) K for the 10% doped compound. The Curie-Weiss temperature of the doped system is also about 80% of that for the pure compound, which is again close to the $(1 - 2x)$ factor describing the decrease of the average number of neighbors of the magnetic ion with doping. On the other hand, even for the 10% doping the $M(T)$ curves demonstrate the same characteristic broad maximum around 35 K as for the pure compound. Thus magnetization measurements prove that the magnetic subsystem of $\text{Li}(\text{Cu}_{1-x}\text{Zn}_x)_2\text{O}_2$ can still be considered as a system of spins ($S = 1/2$) with frustrated exchange interactions, where the spins are arranged in chains along the crystallographic b axis.

According to Ref. 18, the strongest exchange interactions for undoped $\text{Li}(\text{Cu}_{1-x}\text{Zn}_x)_2\text{O}_2$ are the interactions between copper ions within the ab planes: intrachain interactions of nearest spins J_1 , intrachain interactions of next-nearest spins J_2 and interchain interaction J_3 (see Fig. 1). These interactions lead to a spiral long-range magnetic order with an incommensurate wave vector directed along the crystallographic b axis. The solitary nonmagnetic Zn^{2+} defects disturb this spiral magnetic structure in their immediate surroundings only. Since a nonmagnetic defect breaks up nearest-neighbor exchange bonds along the chain but leaves next-nearest exchange bond almost unperturbed, the effect of the solitary defect on the spiral structure can be envisioned as a spiral phase shift at the defect location. Interchain couplings fix relative phases of the neighboring spirals far away from the solitary defect which results in the formation of the disturbed area of the finite size. For small concentrations x , the characteristic size of the disturbed area around nonmagnetic defects can be evaluated as $\frac{2(J_1, J_2)}{J_3}$ cell units, which yields a value of four cell units in the case of LiCu_2O_2 . For $x = 0.1$, the average distance between the defects within the chains amounts to ≈ 5 lattice constants and, therefore the disturbed areas strongly overlap.

As the defect positions in the neighboring chains are uncorrelated, the interchain coupling became frustrated since all interchain bonds obviously can not be satisfied simultaneously because of the spiral phase shift at the defect location. The doped frustrated quasi-one-dimensional system differs significantly from the nonfrustrated doped system: in the case of the nonfrustrated system fragments of the spin chain on the both sides of the defect are decoupled and weak interchain interactions can be completely satisfied by properly setting orientation of the each fragment. Thus, at the strong doping level, long-range order in the frustrated quasi-one-dimensional system is most likely destroyed, while the short-range chiral correlations should persist. We suggest that such a disordered state of the frustrated spin chain can be a realization of a spin-glass-like state with short-range static chiral correlations in the ab planes. The possibility of such state in Zn doped LiCu_2O_2 was suggested earlier by Hsu *et al.*²⁸

The ESR experiments show that the main features of the low-frequency spectrum of excitations in $\text{Li}(\text{Cu}_{1-x}\text{Zn}_x)_2\text{O}_2$ do not change at a doping of $x \leq 0.1$. The spectra can be explained in the frame of a planar spin structure with strong easy-axis anisotropy along the a axis of the crystal. This means that the

spins of this spin-glass like structure lie in the plane defined by the applied magnetic field \mathbf{H} and the axial-anisotropy vector along the a axis for all concentrations x within the entire range $0 \leq x < 0.1$. The absorption linewidth of $\text{Li}(\text{Cu}_{1-x}\text{Zn}_x)_2\text{O}_2$ strongly increases with the Zn concentration (insert in Fig. 5) and the absorption lines of the highly doped samples are asymmetric: the low-field part of the absorption lines is more broadened than the high-field part. Probably, this asymmetry is due to a nonuniformity of the magnetic structure of the doped $\text{Li}(\text{Cu}_{1-x}\text{Zn}_x)_2\text{O}_2$. The defects in the magnetic structure might trigger excitations of magnons with nonzero wave vectors (see, for example, Ref. 30). The resonance condition for such excitations is expected for applied magnetic fields lower than the antiferromagnetic resonance field.

The NMR experiments indicate that the value of the magnetic moments at the position of Cu^{2+} ions at low temperature in doped samples is nearly the same as in the samples without doping at temperatures less than 15 K. Additionally, the shape of the NMR spectra of zinc doped samples indicates short-range static correlations the same as in undoped samples. These correlations appear at the temperature ≈ 18 K, where the anomaly on magnetization curve was observed and the ESR spectra start to be gaped. The temperature evolution of the shape of NMR spectra of doped samples can be explained by appearance of short-range correlations between spins of neighbor ab planes with decrease of the temperature from 9 to 1.8 K. The interpretation of the experimental spectra and our fitting results is natural and one of the simplest, but we can not exclude other models, which can describe the NMR spectra in another way. The results of NMR experiments on strongly doped $\text{Li}(\text{Cu}_{1-x}\text{Zn}_x)_2\text{O}_2$, for $x = 0.1$ are in agreement with the spin-glass-like magnetic structure suggested above.

VI. CONCLUSIONS

Untwinned single-crystalline samples of $\text{Li}(\text{Cu}_{1-x}\text{Zn}_x)_2\text{O}_2$ were grown for $0 \leq x < 0.12$. It is shown that the zinc doping diminishes the number of magnetic copper ions Cu^{2+} and a single crystallographic phase is maintained for all samples within the entire doping range $0 \leq x < 0.12$. The ESR spectra for all doping concentrations within $0 \leq x < 0.12$ can be well explained in the model of a planar spin structure with strong easy-plane type anisotropy for the vector \mathbf{n} normal to the spin plane. The NMR spectra of the highly doped single crystal $\text{Li}(\text{Cu}_{0.9}\text{Zn}_{0.1})_2\text{O}_2$ can be well described by planar spin-glass-like magnetic structure with static short-range spiral correlations. The value of magnetic moments of Cu^{2+} ions in this structure is close to the value obtained for undoped crystals: $(0.8 \pm 0.1) \mu_B$.

ACKNOWLEDGMENTS

We are thankful for the useful and enlightening discussions to S. S. Sosin. This work is supported by the Grant Nos. 12-02-00557-a, 10-02-01105-a, 11-02-92707-IND-a of the Russian Foundation for Basic Research, Program of Russian Scientific Schools, and by the German Research Society (DFG) within the Transregional Collaborative Research Center (TRR 80).

*svistov@kapitza.ras.ru

- ¹T. Hikihara, L. Kecke, T. Momoi, and A. Furusaki, *Phys. Rev. B* **78**, 144404 (2008).
- ²J. Sudan, A. Lüscher, and A. M. Läuchli, *Phys. Rev. B* **80**, 140402(R) (2009).
- ³A. F. Andreev and I. A. Grischuk, *JETP* **60**, 267 (1984).
- ⁴T. Masuda, A. Zheludev, A. Bush, M. Markina, and A. Vasiliev, *Phys. Rev. Lett.* **92**, 177201 (2004).
- ⁵A. A. Gippius, E. N. Morozova, A. S. Moskvina, A. V. Zalessky, A. A. Bush, M. Baenitz, H. Rosner, and S.-L. Drechsler, *Phys. Rev. B* **70**, 020406 (2004).
- ⁶A. A. Bush, V. N. Glazkov, M. Hagiwara, T. Kashiwagi, S. Kimura, K. Omura, L. A. Prozorova, L. E. Svistov, A. M. Vasiliev, and A. Zheludev, *Phys. Rev. B* **85**, 054421 (2012).
- ⁷P. Carretta, A. Rigamonti, and R. Sala, *Phys. Rev. B* **55**, 3734 (1997).
- ⁸S. Liu and A. L. Chernyshev, *Phys. Rev. B* **87**, 064415 (2013).
- ⁹A. Oosawa, T. Ono, and H. Tanaka, *Phys. Rev. B* **66**, 020405(R) (2002).
- ¹⁰D. Hüvonen, S. Zhao, M. Mansson, T. Yankova, E. Ressouche, C. Niedermayer, M. Laver, S. N. Gvasaliya, and A. Zheludev, *Phys. Rev. B* **85**, 100410 (2012).
- ¹¹N. Papinutto, P. Carretta, S. Gonthier, and P. Millet, *Phys. Rev. B* **71**, 174425 (2005).
- ¹²A. Wollny, L. Fritz, and M. Vojta, *Phys. Rev. Lett.* **107**, 137204 (2011).
- ¹³A. Sen, K. Damle, and R. Moessner, *Phys. Rev. Lett.* **106**, 127203 (2011).
- ¹⁴A. Sen, K. Damle, and R. Moessner, *Phys. Rev. B* **86**, 205134 (2012).
- ¹⁵M. Zhitomirsky (private communication).
- ¹⁶H. C. Hsu, J.-Y. Lin, W. L. Lee, M.-W. Chu, T. Imai, Y. J. Kao, C. D. Hu, H. L. Liu, and F. C. Chou, *Phys. Rev. B* **82**, 094450 (2010).
- ¹⁷R. Berger, A. Meetsma, and S. v. Smaalen, *J. Less-Common Met.* **175**, 119 (1991).
- ¹⁸T. Masuda, A. Zheludev, B. Roessli, A. Bush, M. Markina, and A. Vasiliev, *Phys. Rev. B* **72**, 014405 (2005).
- ¹⁹S. Seki, Y. Yamasaki, M. Soda, M. Matsuura, K. Hirota, and Y. Tokura, *Phys. Rev. Lett.* **100**, 127201 (2008).
- ²⁰Y. Kobayashi, K. Sato, Y. Yasui, T. Moyoshi, M. Sato, and K. Kakurai, *J. Phys. Soc. Jpn.* **78**, 084721 (2009).
- ²¹A. Ruydi, I. Mahns, S. Müller, M. Rübhausen, S. Park, Y. J. Choi, C. L. Zhang, S.-W. Cheong, S. Smadici, P. Abbamonte, M. v. Zimmermann, and G. A. Sawatzky, *Appl. Phys. Lett.* **92**, 262506 (2008).
- ²²S. W. Huang, D. J. Huang, J. Okamoto, W. B. Wu, C. T. Chen, K. W. Yeh, C. L. Chen, M. K. Wu, H. C. Hsu, and F. C. Chou, *Sol. State Com.* **147**, 234 (2008).
- ²³L. E. Svistov, L. A. Prozorova, A. M. Farutin, A. A. Gippius, K. S. Okhotnikov, A. A. Bush, K. E. Kamentsev, and É. A. Tishchenko, *JETP* **108**, 1000 (2009).
- ²⁴L. E. Svistov, L. A. Prozorova, A. A. Bush, and K. E. Kamentsev, *J. Phys.: Conf. Series* **200**, 022062 (2010).
- ²⁵A. A. Bush, K. E. Kamentsev, and E. A. Tishchenko, *Inorg. Mater.* **40**, 44 (2004).
- ²⁶A. M. Vorotynov, A. I. Pankrats, G. A. Petrakovski, K. A. Sablina, V. Pashkovich, and G. Shimchak, *JETP* **86**, 1020 (1998).
- ²⁷Antiferromagnetic resonance of the planar spiral spin structure is discussed in Ref. 23 and in the arXiv:1304.4728.
- ²⁸H. C. Hsu, W. L. Lee, J.-Y. Lin, H. L. Liu, and F. C. Chou, *Phys. Rev. B* **81**, 212407 (2010).
- ²⁹The value of the chemical shift, as determined in our experiments at the paramagnetic phase ($T = 29$ K), is equal to 0.075 ± 0.005 T/ μ_B at $\mathbf{H} \parallel \mathbf{c}$.
- ³⁰H.-A. Krug von Nidda, L. E. Svistov, and L. A. Prozorova, *Low Temp. Phys.* **36**, 736 (2010), arXiv:1006.5192.